ICARUS 59, 462–477 (1984)

Impact Fragmentation Experiments of Basalts and Pyrophyllites

YASUHIKO TAKAGI, HITOSHI MIZUTANI, AND SHIN-ICHI KAWAKAMI

Department of Earth Sciences, Nagoya University, Nagoya, 464, Japan

Received October 13, 1983; revised March 2, 1984

Results of impact fragmentation experiments for basalts and pyrophyllites are reported. Aluminum cylindrical projectiles were impacted on cubic basalt and pyrophyllite targets at velocities of 70 to 990 m/sec. The targets and projectiles were 20 g to 3.3 kg and 2 to 20 g in weight respectively. Weights of the fragments produced by impacts were measured and the size distributions of fragments were examined. Data of the largest fragment mass (m_L) normalized to the original target mass (M_t), m_L/M_t, correlate better with the nondimensional impact stress, P_1, a new scaling parameter introduced by H. Mizutani, Y. Takagi, and S. Kawakami (1984, in preparation) than the conventional projectile's kinetic energy per unit target mass, E/M_t, used in the previous studies. All the m_L/M_t data for basalts obtained in the present study are summarized by $m_L/M_t = 2.95 \times 10^{-2} P_1^{-1}$, where $P_1 = P_0 L^3/YR^3$, P_0 = peak shock pressure, L = projectile size, R = target size, and Y = material strength of target. For aluminum targets, however, the m_L/M_t is 2.5 orders of magnitude larger than that for brittle targets at impacts with the same P_1. Size distributions of fragments expressed in a log N − log (m/M_t) diagram are divided into three regimes bounded by two inflection points. In each regime the curve is expressed by $N(>m/M_t) = A(m/M_t)^{-a}$. The slopes, a, of the log N − log (m/M_t) curves in the regimes of a large and a medium size range are positively correlated with the nondimensional impact stress, P_1, and expressed as $a = C_3 + a_3 \log P_1$. The slopes, a, in the smallest size range are, on the other hand, nearly constant and have values of 0.5 to 0.7 ($\frac{1}{2}$–$\frac{2}{3}$). Present results indicate that the impact fragmentation is scaled well by the new scaling parameter, P_1, of Mizutani, Takagi, and Kawakami and that the present experimental data may shed new light on planetary impact processes.

INTRODUCTION

It is generally considered that various types of impacts of solid bodies had occurred in the history of the solar system and that these phenomena significantly influenced formation and evolutional process of planets. Many experimental studies were performed to elucidate the nature of planetary impact phenomena. Most of them, however, had been cratering experiments where a small projectile is impacted with a high velocity on a very large target.

Understanding of impact fragmentation as well as impact cratering, however, is important to consider planetary formation process in the early history of the solar system, because accretional processes of protoplanets and planets heavily depend on the ease of impact fragmentation of these bodies. Only a few experimental studies intending to clarify the impact fragmentation process have been made so far. Catastrophic impacts at high velocities were studied by Gault and Wedekind (1969), Fujiwara *et al.* (1977), and Fujiwara and Tsukamoto (1980), and those at lower velocities by Hartmann (1978) and Matsui *et al.* (1982). Basalt targets were studied by Fujiwara *et al.* and Fujiwara and Tsukamoto in the velocity range of 2500–2900 m/sec and by Matsui *et al.* in the velocity range of 50–150 m/sec. Since the velocity ranges used by the above two groups have a gap larger than an order of magnitude, it is desirable to bridge the gap by making additional impact experiments for basalt in the intermediate velocity range.

In the present study we made impact experiments on basalts and pyrophyllites in a rather wide range of impact velocity (V_i = 70–990 m/sec) in order to understand the

0019-1035/84 $3.00

impact process on rocks more fully. Now that we have the four data sets of impact experiments on basalt targets made in different velocity ranges by three different groups, combination of these data should reveal a well-defined picture of impact phenomena.

Studies comparable to the present one were made for ice targets by Lange and Ahrens (1981, 1982) and Kawakami *et al.* (1983). Since the strength of ice is orders of magnitude smaller than that of basalts, comparison of the present results with those for ice is useful to clarify the strength effects of impact fragmentation.

Mizutani *et al.* (1984) gave a new scaling law on impact fragmentation on the basis of their recent scaling parameter, called the "late-stage effective energy" (Mizutani *et al.*, 1983). In the present paper, we describe the experimental data and discuss them in terms of the scaling law of Mizutani *et al.* The result seems to verify the general validity of their scaling law.

EXPERIMENTAL PROCEDURE

The present impact experiments were made by using the single-stage powder gun facility at the Department of Earth Sciences, Nagoya University (Mizutani *et al.*, 1981). The gun has a novel sabot stopper device described in Mizutani *et al.* (1981) and is used for firing a variety of size of projectiles. Ambient pressure in the target chamber was always maintained at about 20 Pa.

The samples used as targets were fine-grained basalts and very homogeneous natural pyrophyllites. Some pertinent information on physical and other properties of the samples used in the present paper is listed in Table I. The strength of the basalts and pyrophyllites used in the present study and the basalts used in Fujiwara *et al.* (1977) was measured with a uniaxial testing machine at a strain rate of $\dot{\varepsilon} = 10^{-4}$/sec in our laboratory (Table I). The uniaxial compressive strength of the basalt used here (Y = 480 MPa) is significantly larger than those

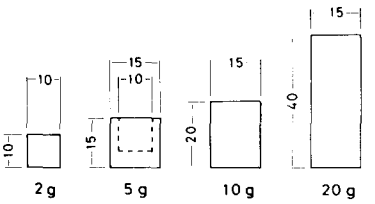

FIG. 1. Various shapes of aluminum projectiles used in this study. The numbers in the figure indicate lengths in mm.

of basalts used by Fujiwara *et al.* (Y = 160 MPa) and Matsui *et al.* (Y = 220 MPa). The strength of pyrophyllite used is 73 MPa, which is about a factor of 7 smaller than those of basalts. Targets of both the basalt and the pyrophyllite were 20 g to 3.2 kg in weight and cubic in shape with edge lengths of 2 to 10 cm. Although most of the target material was very homogeneous and did not contain any visible cracks, samples 820730 and 820802 contained rather large cracks near the surface. Therefore the experiments for these two samples should be treated with some caution.

Targets were suspended in a recovery box of transparent acryls by cotton threads. The inner walls of the box were covered by thick urethane-foam sheets to prevent fragments from being refragmented at collisions on the walls.

We used aluminum 2017B as projectiles. The mechanical properties of the aluminum are also listed in Table I. Projectiles were cylindrical in shape, 2 to 20 g in weight, 10 and 15 mm in diameter, and 10 to 40 mm in length. Slightly different shapes of projectiles depending on their masses were used and are shown in Fig. 1. The length-to-diameter ratios (L/D) of most projectiles are about 1, though the ratios for projectiles with M_p = 20 g are significantly different from 1, and the upper ends of the projectiles with M_p = 5 g are hollowed. The difference in shape among projectiles may invalidate the similarity of flow field and thus may obscure the scaling law to be explored. In the following discussion of the scaling law, we omit the data for the projectiles

TABLE I

MECHANICAL PROPERTIES OF MATERIALS USED IN THE PRESENT PAPER

Material	Density (kg/m^3)	Compressive strength (MPa)	Compressional wave velocity (m/sec)	Shear wave velocity (m/sec)	Young's modulus (GPa)	Poisson's ratio	Bulk sound velocity (m/sec)	s[a]
			Target					
Basalt (Chausu-yama, Japan)	2818 ± 2	480	6480 ± 120	3530 ± 130	90.5	0.29	5040	1.25
Pyrophyllite (USA)	2711 ± 8	73	3990 ± 50	2280 ± 120	35.4	0.26	3000	1.25
Basalt (Yakuno, Japan)[b]	2615 ± 10	160	4640 ± 140	2930 ± 280	53.2	0.17	3170	1.25
Basalt (Kinosaki, Japan)[c]	2720 ± 10	220	4370 ± 40	2600 ± 60	45.1	0.23	3180	1.25
			Projectile					
Al 2017B	2785	300[d]	6420	3040	69.9	0.36	5370	1.338
Polycarbonate[b]	1300						2847	1.404
Mild Steel CK15[c]	7940		5960	3240	215	0.29	4640	1.92

[a] $s = \{(\partial K/\partial P)_T + 1\}/4$ where K is the bulk modulus.
[b] Materials used in Fujiwara *et al.* (1977) and Fujiwara and Tsukamoto (1980).
[c] Materials used in Matsui *et al.* (1982).
[d] Tensile yield strength.

with M_p = 20 g. But we will not omit the data for projectiles with M_p = 5 g, because the data for projectiles with M_p = 5 g are quite consistent with the data obtained for solid cylinders of L/D = 1 with similar impact velocities (e.g., 830513, 840111, 840113). Therefore we assume here that the hollowed projectiles with M_p = 5 g do produce impact flow fields similar to those produced by solid cylinders of L/D = 1.

The impact velocity range in the present study was 70 to 990 m/sec. Experimental conditions for individual runs are listed in Table II. Impact velocities used in the present study are larger than those in Matsui *et al.* (1982) but smaller than those in Fujiwara *et al.* (1977) and Fujiwara and Tsukamoto (1980). The maximum kinetic energy in the present studies, on the other hand, exceeds those in the previous studies listed above.

Recovered fragments were sorted out by standard meshes. Fragments larger than 2.83 mm were weighed individually. Fragments on each mesh larger than 1.00 mm in mesh size were counted but only the total weight of the fragments was recorded: fragments were assumed to be of equal weight and the individual weight was obtained by dividing the total weight of the fragments by the number of fragments counted. For fragments smaller than 1.00 mm in mesh size, we weighed only the total mass of fragments left on each sieve and the number of fragments was estimated by assuming each fragment to be a sphere. Because the fragment left on a particular mesh is larger than the mesh size and smaller than that of the one-step-coarser mesh (with $\sqrt{2}$ times larger size), the diameter of the assumed sphere is taken to be the mean size of the two mesh sizes. Differences in the methods of counting fragments among the different size ranges do not seem to affect the results significantly, for the resultant N(number)–m(mass) curves for the fragments show no inflection at the boundaries of the counting methods. A detailed comparison of the various counting methods is given in Takagi (1983). Fragments counted in a single run numbered 50 to 50,000.

RESULTS

Mode of Destruction

The mode of destruction of targets observed in this study is classified in the order of decreasing impacted specific energy of the impact into four types: (1) rebound of projectile with no cratering, (2) cratering, (3) cone destruction or longitudinal splitting, and (4) complete destruction type as observed in previous studies (Fujiwara *et al.*, 1977; Matsui *et al.*, 1982; Lange and Ahrens, 1981). We could not observe core-type destruction where the central part of a target survives at impact as reported by Fujiwara *et al.* (1977) and Gault and Wedekind (1969) for impacts at high velocity ranges and small M_p/M_t ratios. As noted by Matsui *et al.* (1982), slow-velocity impacts with specific energies as large as those corresponding to the core-like fragmentation of Fujiwara *et al.* (1977) did produce the cone-like fragmentation. In this mode, fragments from four rear side corners of a target have nearly the same masses and cone-like shapes whose peaks are toward the center of the impact point. The difference in the mode of fragmentation between the present result and the result of Fujiwara *et al.* must be related to the difference in impact velocity and M_p/M_t ratio between our experiments and theirs. The discrepancy observed in the fragmentation mode indicates that the mode of fragmentation is not a sole function of the specific impact energy but may be a rather complex function of impact velocity and M_p/M_t ratio. The new scaling factor by Mizutani *et al.* (1984), which successfully explains the size distribution of fragments of various experiments, is not useful in delineating the mode of fragmentation. Probably, detailed information on impact pulse and pulse propagation may be required to explain the difference in fragmentation mode observed between low-velocity ($v < 1$ km) and high-velocity ($v > 1$ km) experiments.

TABLE II

EXPERIMENTAL CONDITIONS

Run No.	Projectile mass (g)	Target mass (g)	Impact velocity (m/sec)	Impact energy (kJ)	Peak stress (GPa)	Late-stage effective energy (kJ)	P_1	Recovery rate (%)	
				Basalt target					
820117	4.96	126.58	820	1.67	6.58	11.8	0.544	95	(A)[a]
820125	4.96	415.3	862	1.84	6.95	12.3	0.175	98	(B)
820219	5.02	1056.8	820	1.69	6.58	11.8	0.066	100	(C)
820517	4.99	49.17	820	1.68	6.58	11.8	1.408	86	(D)
820518	4.51	19.48	855	1.65	6.89	11.2	3.362	81	(E)
820519	10.05	32.81	641	2.06	5.04	18.2	3.254	85	(F)
820520	9.98	404.8	599	1.79	4.69	16.8	0.244	96	(G)
820521	9.98	1048.8	600	1.80	4.70	16.9	0.094	100	(H)
820523	10.00	159.29	289	0.417	2.18	7.83	0.289	96	(I)
8205261	10.30	46.96	269	0.372	2.03	7.51	0.939	95	(J)
8205262	10.21	22.88	135	0.0935	1.00	3.67	0.941	100	(K)
820527	10.24	346.8	134	0.0922	0.992	3.65	0.059	100	(L)
820528	10.21	109.04	136	0.0942	1.01	3.71	0.199	100	(M)
820602	10.22	446.4	275	0.386	2.07	7.60	0.100	100	(N)
820603	5.02	3220	813	1.66	6.52	11.7	0.021	100	(O)
820610	20.04	22.23	93.2	0.0870	0.687	4.94	1.306	100	(P)
820611	20.25	139.40	94.7	0.0908	0.698	5.07	0.214	100	(Q)
820702	10.30	47.18	135	0.0935	1.00	3.69	0.460	100	(R)
820721	10.91	32.44	70	0.0267	0.514	2.02	0.364	99	(S)
820723	11.40	18.06	123	0.0826	0.910	3.72	1.211	93	(T)
820724	5.11	104.91	990	2.50	8.1	14.6	0.832	92	(U)
820730	10.16	45.39	140	0.0996	1.04	3.95	0.491	100	(V)
820802	10.21	96.29	127	0.0823	0.940	3.45	0.210	100	
820810	10.14	210.20	279	0.393	2.10	7.64	0.214	100	(X)
820812	10.21	28.73	303	0.469	2.29	8.39	1.716	94	(Y)
820825	10.18	99.04	280	0.399	2.11	7.71	0.457	100	(Z)
820829	10.13	36.88	658	2.19	5.19	18.9	3.005	88	(a)
820830	10.18	34.25	629	2.01	4.94	18.0	3.095	82	(b)
820831	10.22	31.97	645	2.12	5.08	18.6	3.423	84	(c)
820907	10.21	30.39	119	0.0723	0.880	3.20	0.623	100	(d)
820908	5.05	46.56	820	1.70	6.58	12.0	1.505	94	(e)
820918	10.24	59.24	135	0.0933	1.00	3.68	0.364	98	(f)
821013	10.11	158.19	280	0.396	1.25	7.66	0.284	99	(g)
821216	10.40	408.4	613	1.95	4.81	17.9	0.258	100	(h)
830119	10.34	51.63	272	0.382	2.05	7.61	0.866	98	(i)
830125	10.15	289.4	629	2.01	4.94	18.0	0.365	98	(j)
830513	2.23	181.15	714	0.568	5.66	4.53	0.147	100	(k)
840111	2.18	14.89	662	0.478	5.22	4.05	0.476	98	(n)
840113	7.09	219.11	920	3.00	7.47	18.8	0.504	84	(m)
				Pyrophyllite target					
8111192	2.22	596.9	290	0.0934	1.62	1.30	0.080	100	
8111241	2.22	591.4	950	1.00	5.93	4.73	0.297	99	
8111261	2.22	589.4	700	0.544	4.20	3.35	0.211	99	
8201071	2.22	589.4	525	0.306	3.06	2.44	0.154		
830115	10.32	585.3	581	1.74	3.41	12.6	0.802	94	
830325	10.12	594.9	641	2.08	3.81	13.7	0.864	98	
830506	10.01	599.2	258	0.333	1.43	5.09	0.319	100	
830617	10.06	198.11	620	1.93	3.67	13.2	2.485	92	

[a] The last column represents labels in Fig. 8.

TABLE III

SUMMARY OF THE EXPERIMENTAL RESULTS

Run No.	Slope			Largest fragment mass (m/Mt)
	Regime I	Regime II	Regime III	
		Basalt target		
820117	1.88	0.74	0.56	0.0874
820125	0.98	0.68	0.54	0.0861
820219	0.66	0.36	0.53	0.361
820517	1.92	0.84	0.58	0.0248
820518	3.73	0.93	0.95	0.0067
820519	2.60	1.18	0.80	0.0134
820520	1.40	0.84	0.58	0.0744
820521	1.02	0.42	0.50	0.217
820523	1.45	0.43	0.52	0.111
8205261	2.44	0.83	0.66	0.0187
8205262	2.33	0.62	0.62	0.0468
820527	0.16	0.32	0.60	0.961
820528	0.74	0.25	0.57	0.601
820602	0.72	0.23	0.53	0.438
820603	0.25	0.38	0.70	0.888
820610	1.92	0.67	0.55	0.256
820611	0.17	0.47	0.60	0.585
820702	1.33	0.39	0.45	0.210
820721	2.56	0.43	0.49	0.151
820723	3.49	0.98	0.60	0.038
820724	2.53	1.23	0.69	0.014
820730	2.01	0.46	0.38	0.505
820802	1.01	0.29	0.40	0.497
820810	1.11	0.34	0.40	0.221
820812	3.30	1.27	0.74	0.0207
820825	2.25	0.85	0.51	0.0407
820829	3.95	1.23	0.93	0.0079
820830	3.08	1.43	1.15	0.0092
820831	3.49	1.35	0.90	0.0066
820907	2.23	0.44	0.47	0.0865
820908	2.10	1.19	0.71	0.0268
820918	1.28	0.43	0.55	0.153
821013	2.61	0.90	0.45	0.0464
821216	4.70	0.93	0.49	0.0378
830119	2.05	1.28	0.70	0.0139
830125	2.14	1.11	0.70	0.0257
830513	0.73	0.47	0.51	0.219
840111	2.71	1.00	0.66	0.185
840113	1.61	0.99	0.64	0.0329
		Pyrophyllite target		
8111192	0.21	0.27	0.90	0.947
8111241	2.0	0.55	0.47	0.0989
8111261	1.1	0.27	0.55	0.236
8201071	0.89	0.16	0.61	0.44
830115	2.90	0.87	0.62	0.0645
830325	1.48	0.81	0.60	0.0593
830506	0.90	0.47	0.55	0.319
830617	2.61	0.93	0.73	0.0224

The Largest Fragment Mass

As suggested by Gault and Wedekind (1969), Fujiwara *et al.* (1977), and Hartmann (1978), the mass of the largest fragment normalized by the original target mass (m_L/M_t) is a useful parameter to denote the degree of impact fragmentation. The m_L/M_t ratios obtained in each experiment of the present study are listed in Table III. As in the previous studies (Gault and Wedekind, 1969; Fujiwara *et al.*, 1977; Fujiwara and Tsukamoto, 1980; Matsui *et al.*, 1982), we plotted m_L/M_t ratios against the projectile's kinetic energies per unit target mass in Figs. 2 and 3. As shown in these figures, m_L/M_t ratios from our experimental results for basalt and pyrophyllite are approximately expressed by

$$m_L/M_t = C_1(E/M_t)^{-a_1} \qquad (1)$$

where m_L is the mass of the largest fragment, M_t is the mass of a target, E is the kinetic energy of projectile, and C_1 and a_1 are constants. The constants obtained by the least-squares fittings of the present ex-

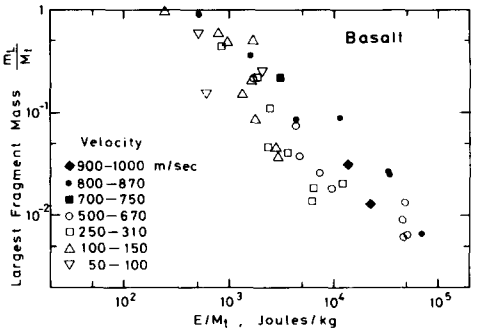

FIG. 2. The largest fragment mass normalized by the original target mass for the basalt target versus the specific kinetic energy of the projectile.

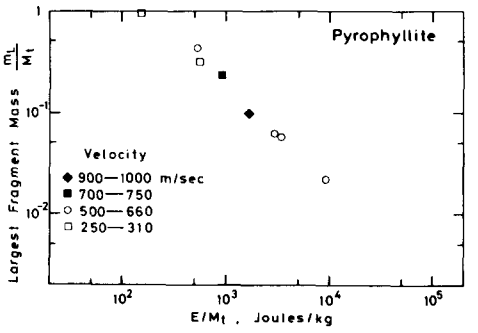

FIG. 3. The largest fragment mass normalized by the original target mass for the pyrophyllite versus the specific kinetic energy of the projectile.

TABLE IV

RESULTS OF THE LEAST-SQUARES FITTING OF THE EXPERIMENTAL DATA ON LARGEST FRAGMENT SIZE WITH EQS. (1) AND (9)

		$(m_L/M_t) = 10^{C_1}(E/M_t)^{-a_1}$		
		C_1[a]	a_1[a]	σ[b]
Present study	Basalt	2.08 (0.27)	0.89 (0.07)	0.28
	Pyrophyllite	2.12 (0.13)	0.95 (0.04)	0.06
Fujiwara *et al.*	Basalt	3.26 (0.36)	1.24 (0.10)	0.28
Matsui *et al.*	Basalt (cubic)	3.37 (1.24)	1.53 (0.58)	0.27
All basalt data		1.90 (0.21)	0.86 (0.06)	0.32
		$(m_1/M_t) = 10^{C_2} P_1^{a_2}$		
		C_2[a]	a_2[a]	σ[b]
Present study	Basalt	−1.53 (0.06)	1.00 (0.09)	0.37
	Pyrophyllite	−1.23 (0.08)	1.08 (0.13)	0.14
All basalt data		−1.54 (0.06)	0.92 (0.08)	0.38

[a] Numbers in parentheses are standard deviations of the estimated parameters.

[b] $\sigma = \sqrt{\Sigma\{\log(m_1/M_t)_{exp} - \log(m_L/M_t)_{theor}\}^2/N}$.

perimental data on basalt and pyrophyllite are given in Table IV. The good agreement of constants C_1 and a_1 between basalt and pyrophyllite is remarkable but it may be coincidental in view of the quite different mechanical properties between basalt and the pyrophyllite. As we will show later, the coincidence may be due to the combination of the opposite effects of material strength and impact velocity on impact fragmentation: the average impact velocity for pyrophyllite targets is larger by about 150 m/sec than that for basalt targets. The constants a_1 obtained here should be compared with those in the equations of Fujiwara *et al.* (1977),

$$m_L/M_t \propto (E/M_t)^{-1.24}, \quad (2)$$

and Matsui *et al.* (1982)

$$m_L/M_t \propto (E/M_t)^{-1.53}, \quad (3)$$

both of which were obtained for cubic basalt targets. The present value of the exponent a_1 is smaller than those in Eqs. (2) and (3) but the difference may not be significant because the data obtained by the three groups scatter rather widely as shown in Fig. 4. If we fit all the experimental data available for basalts obtained by the three independent groups to Eq. (1), we obtained the parameters listed in the fifth row of Table IV. Comparison of the data obtained in the present study with the experiments of Matsui *et al.* for basalts indicates that the (m_L/M_t) versus (E/M_t) curves shift to the right as the impact velocity increases. But the data of Fujiwara *et al.* do not fall into

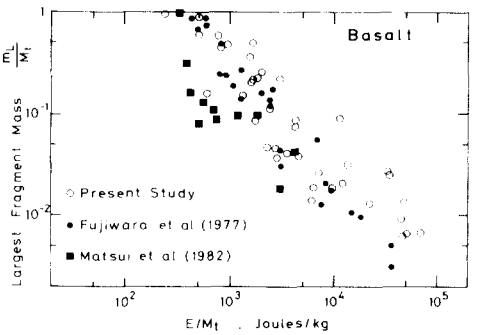

FIG. 4. Comparison of experimental data obtained by three independent groups on the largest fragment mass of basalts normalized by the original target mass versus the specific kinetic energy of the projectile.

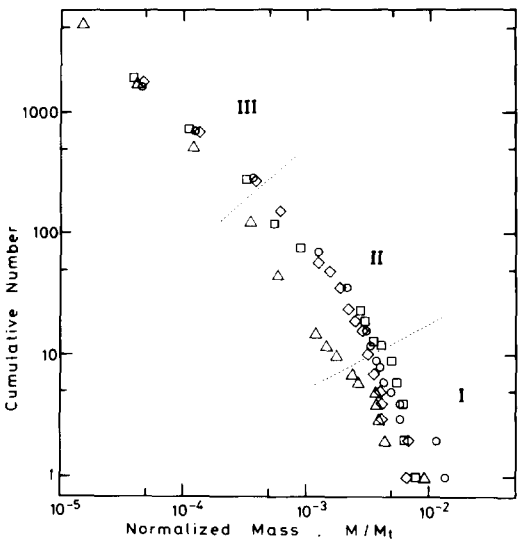

FIG. 5. Four size distributions of fragments from the impact experiments performed for basalt targets under nearly same conditions (V = 640 m/sec, M_t = 35 g, and M_p = 10 g).

the rightmost region of the diagram as expected, in spite of their high velocity (v = 2600 m/sec). As will be discussed later, the deviation of the data of Fujiwara *et al.* from the general trend of the velocity dependence of the constant C_1 may be related to the very low strength of their basalts: the compressive strength of our samples is 480 MPa, whereas that of the sample of Fujiwara *et al.* is only 160 MPa.

The experimental data given in Figs. 2 and 3 and the above discussion show that the mass of the largest fragment is not properly expressed by Eq. (1): the constants C_1 and a_1 in Eq. (1) seem to depend on the impact velocity and strength of rocks. In a later section we will describe an alternative equation which can represent the experimental data much better in a wide range of impact velocity and strength of rocks.

Size Distribution of Fragments

Four experiments (820518, 820829, 820830, and 820831) were performed under nearly identical conditions to test the reproducibility of the experimental results. Projectiles 10.1 ± 0.1 g in weight were impacted on basalt targets 34.5 ± 2.5 g in weight at impact velocities of 643 ± 15 m/sec. The size distributions of the impact fragments from the four experiments are shown in Fig. 5. Although the impact fragmentation is a highly transient phenomenon, the results indicate that the size distributions of fragments are very reproducible. Even the mass of the largest fragments, which are thought to be the most erratic in nature, coincide with each other within a factor of 2. The scatter of the data points in Fig. 5 is probably due to sample heterogeneity, slight deviation from normal incidence of a projectile, and other factors which were not controlled in the present experiments. Therefore any theoretical and/or empirical prediction of the size distribution must allow for scatter of this magnitude, and would be sufficient if it could predict the size distribution within the scatter.

Figure 6 shows the size distributions of fragments destroyed by 5-g projectiles at velocities of about 820 m/sec. The targets varied from 3.32 kg to 49 g in weight. The largest fragment mass normalized by the original target mass decreases and the slope of the N (cumulative number of fragments) $- m/M_t$ curves in the large mass range increases as the target mass decreases.

Figure 7 shows data complementary to those shown in Fig. 6. Here, target and projectile masses are held constant (M_p = 10 g and M_t = 405 ± 40 g), but impact velocities are varied from 134 to 599 m/sec. The general trend of the $N - m/M_t$ curves is about the same as that in Fig. 6: as the intensity of the impact increases, the normalized mass of the largest fragment decreases and the slope of the curves increases.

Observing the data in Figs. 6 and 7, we notice that every size distribution curve has two inflection points. The size distributions are divided into three regimes by these inflection points. We call these regimes "regime I," "regime II," and "regime III" in order of decreasing mass of fragments. Re-

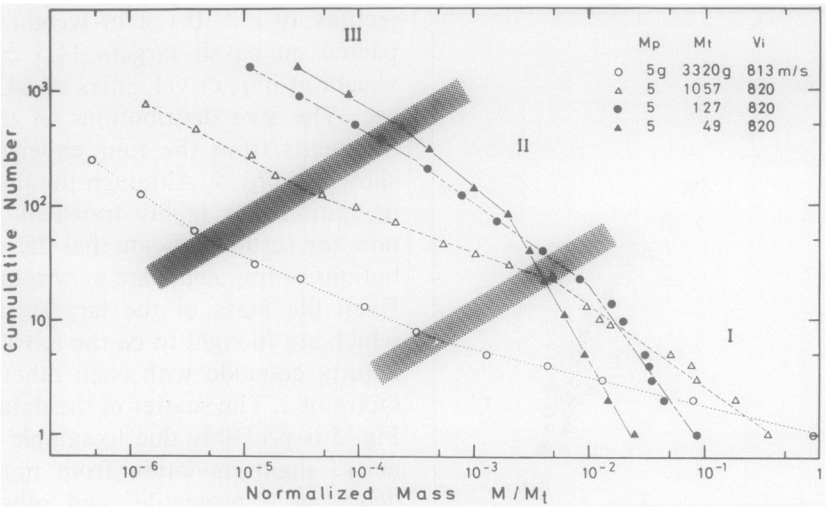

FIG. 6. Size distributions of the basalt fragments from targets with different masses destroyed by 5-g projectiles at velocities of about 820 m/sec.

gime I covers the size range from the largest fragments to 10^{-2}–$10^{-3}M_t$ fragments. Regime III covers the size range of fragments smaller than 10^{-5}–$10^{-3}M_t$. Regime II is the intermediate regime. In each regime, the size distribution curve is denoted by the well-known power law

$$N(>m) = Am^{-a} \qquad (4)$$

where $N(>m)$ is the cumulative number of fragments heavier than m, and A and a are constants. Each size distribution of fragments in all of the present data is well represented by three equations of the Eq. (4) type. In Fig. 8 are shown the size distributions of basalt fragments, obtained by fitting Eq. (4) into each regime to all experimental data reported in the present paper. The in-

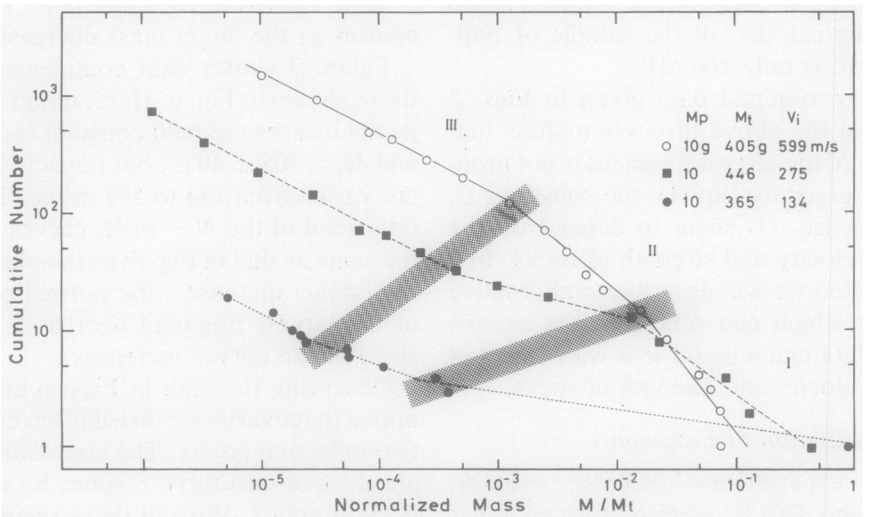

FIG. 7. Size distributions of basalt fragments from targets of about 400 g in weight destroyed by 10-g projectiles at various impact velocities.

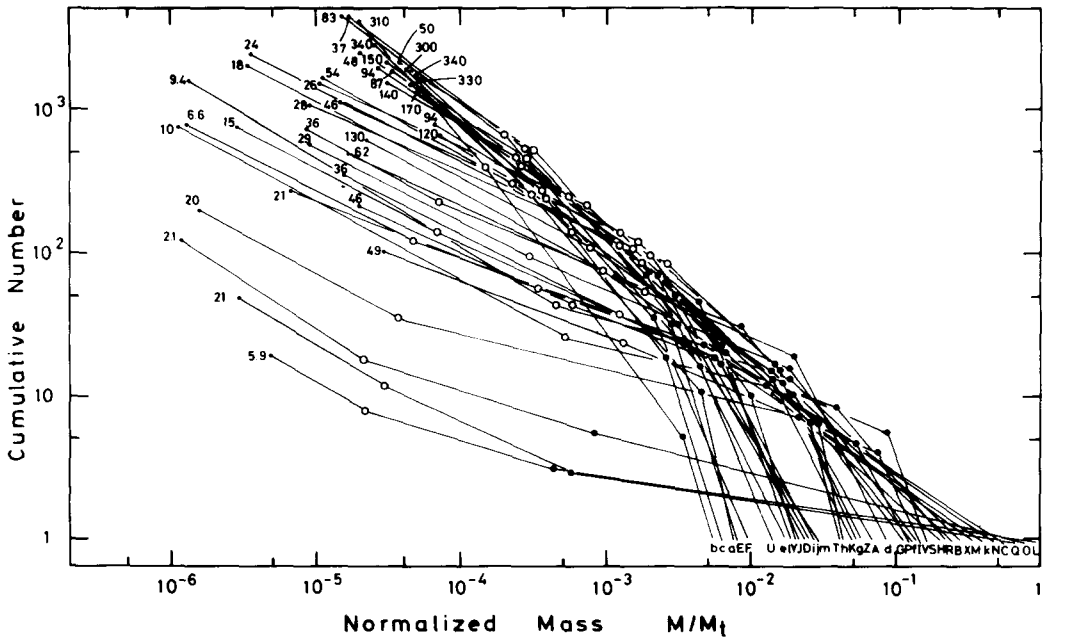

FIG. 8. Summary of all size distributions of basalt fragments obtained in the present experiments by fitting Eq. (8) in each regime. Numbers attached to curves indicate the nondimensional impact stress multiplied by 100 ($100P_I$) of the impact by which the fragments of the size distribution were made. Closed circles and open circles show inflection points from regime I to II and from regime II to III, respectively. Labels at the lower right are listed in the last column of Table II.

flection points from regime I to II are shown by solid circles and those from regime II to III are shown by open circles. The zone which the inflection points occupy takes an inclined Λ shape but its physical significance is not clear at the present stage.

SCALING LAW OF IMPACT FRAGMENTATION

Maximum Size Fragment

Mizutani *et al.* (1983) found that diameters of craters excavated in sand are expressed systematically by the "late-stage effective energy" at all velocity ranges but not by the impact kinetic energy. The late-stage effective energy is a natural extension of the "late-stage equivalent momentum" of Dienes and Walsh (1970) and takes the form

$$I = M_p P_0/\rho_{0p} \tag{5}$$

where ρ_{0p} is the zero-pressure density of the projectile and P_0 is the peak pressure generated at an impact. The impact peak pressure, P_0, is calculated in the standard manner (e.g., Rinehart, 1975; McQueen *et al.*, 1970) using the Hugoniot relation approximated by the well-known equation

$$U = C + su \tag{6}$$

where U is the shock wave velocity, u is the particle velocity, and C and s are constants. The values of C and s used in the present study are listed in Table I. The values of C for basalt and pyrophyllite were estimated from the ultrasonically determined compressional- and shear-wave velocities V_p and V_s using the equation (Ruoff, 1967; McQueen *et al.*, 1970)

$$C^2 = V_p^2 - \tfrac{4}{3}V_s^2. \tag{7}$$

Constants s for basalt and pyrophyllite were assumed to be $\frac{5}{4}$, which corresponds

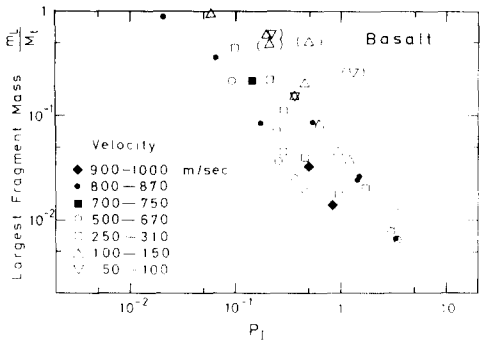

FIG. 9. The largest fragment mass normalized by the original target mass of basalt target experiments versus the nondimensional impact stress, P_I. Inverse triangles in parentheses represent experiments with 20-g projectiles which have significantly larger length/diameter ratios than others. Triangles in parentheses represent experiments for basalt targets with preexisting cracks. These four data were not included in the least-squares fitting of Eq. (9).

to the common value, $(\partial K/\partial P)_T = 4$, because s is approximately equal to $\{(\partial K/\partial P) + 1\}/4$ (Ruoff, 1967).

Many previous workers have interpreted their data on impact fragmentation in terms of the specific kinetic energy, E/M_t. Recently Mizutani *et al.* (1984) proposed a general scaling law for impact fragmentation phenomena using the late-stage effective energy. According to their scaling law, the largest fragment mass normalized to the original target mass, m_L/M_t, should be scaled by their new parameter, P_I, which is defined by the equation

$$P_I = I\rho_t/M_t Y \tag{8a}$$

or

$$P_I = P_0 V_{0p}/Y V_{0t} \tag{8b}$$

where I is the late-stage effective energy, ρ_t is the density of a target, M_t is the mass of a target, Y is the material strength of a target, P_0 is the impact pressure, and V_{0p} and V_{0t} are the initial volumes of a projectile and a target, respectively. The parameter P_I corresponds to the ratio of the shock–stress amplitude at the target's rear surface to the material strength. For a discussion of impact fragmentation, it may be appropriate to use the tensile strength at a high strain rate as the material strength in Eq. (8). But we will use the compressive strength instead of the tensile strength, because the compressive strength is easier to measure in our laboratory. According to the Griffith (1920) theory on fracture, the compressive strength in a brittle material is eight times larger than the tensile strength. Experimental data for many rocks indicate that the ratios of compressive strength to tensile strength are about 10 to 20 and that they could be considered to be rather constant and independent of rock type (Paterson, 1978). As long as the ratio of compressive strength to tensile strength is constant, use of the compressive strength in Eq. (8) is immaterial in the present discussion.

Figures 9 and 10 show m_L/M_t values obtained in the present experiments on basalt and pyrophyllite targets against P_I respectively. Least-squares fitting of the data by the equation

$$m_L/M_t = C_2 P_I^{-a_2} \tag{9}$$

gives the parameters of C_2 and a_2 listed in Table IV. Comparison of the coefficients of Eqs. (1) and (9) listed in Table IV indicates that the standard deviations of the m_L/M_t–P_I relations are as small as those of the m_L/M_t–E/M_t relations. It is noteworthy here that the exponents of a_2 for both basalt and pyrophyllite are very close to 1, which may

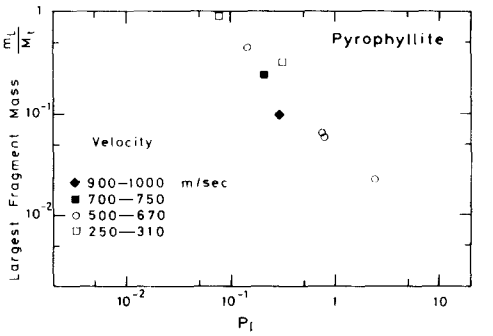

FIG. 10. The largest fragment mass normalized by the original target mass of the pyrophyllite target versus P_I.

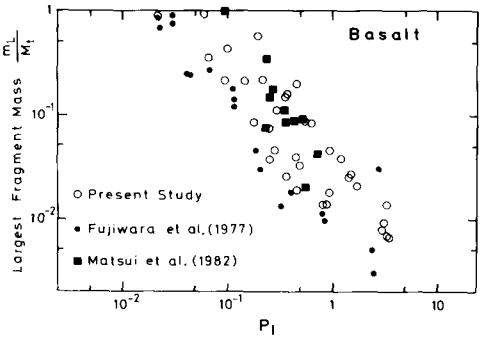

FIG. 11. All data on largest fragment mass normalized by the original target mass for basalt versus P_I obtained by three independent groups.

indicate the physical significance of the parameter, P_I, in the impact fragmentation.

In Fig. 11, we plotted all of the m_L/M_t data for basalts against P_I (Fujiwara *et al.*, 1977; Matsui *et al.*, 1982). The parameters, P_I, for the experimental data by Fujiwara *et al.* (1977) and Matsui *et al.* (1982) were also calculated by the same procedure used for our experimental data. The pertinent data used are given in Table I. Impact velocities in the Fujiwara *et al.* experiments are larger than those of Matsui *et al.* by two orders of magnitude. All data in Fig. 11 are clustered fairly tightly around the line in Fig. 9, in spite of the large differences in impact velocities, M_p/M_t ratios, and strengths.

The coefficient and exponent of Eq. (9) obtained by the least-squares fittings of all data for basalts are also given in Table IV. Although the standard deviation of the fitting error by Eq. (9) is not significantly smaller than that by Eq. (1), this magnitude of the standard deviation might be inevitable, because the original data for m_L/M_t contain rather large scatters even for impacts made under identical conditions and the estimated P_I values contain some uncertainties for parameters such as C, s, and Y. Although the new parameter, P_I, cannot be concluded to be a much better scaling parameter than the specific kinetic energy from the present data alone, several other lines of evidence (Mizutani *et al.*, 1984) including the size distributions of fragments described in the following section show that the parameter, P_I, is the best scaling parameter proposed so far.

The validity of the present scaling parameter, P_I, is demonstrated by comparing the size distributions of fragments produced in some experiments with almost the same P_I values. In Fig. 12, we show the size distributions of fragments obtained for three groups of experiments with P_I = 1.7–2.5, 0.29–0.30, and 0.06–0.08 respectively. Although the impact velocities and the specific kinetic energies are different by more than a factor of 2 in each group of experiments, the size distributions of fragments including the m_L/M_t ratios in each group are very similar to each other. These observations suggest that the impact fragmentation is better scaled by the present parameter, P_I, than the specific kinetic energy.

The mass of the largest aluminum fragment imparted from the projectile normalized to the original projectile mass, m_L/M_p, is plotted as a function of P_I in Fig. 13. The tensile yield strength, 300 MPa, is used as the strength of the aluminum. The data in Fig. 13 indicate that fragmentation of aluminum requires a P_I 2.5 orders of magnitude larger than that required for basalt fragmentation. If we use the spall strength of 973 MPa obtained by Gehring (1970) as the strength of aluminum, the difference in P_I between aluminum and basalt becomes two

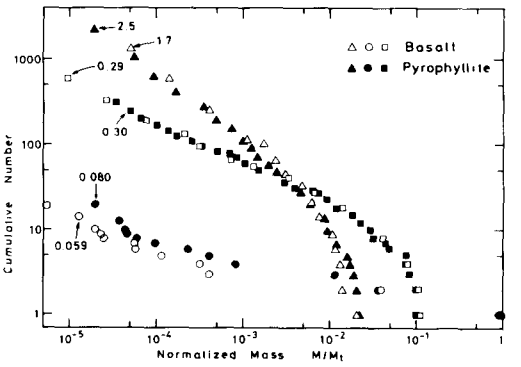

FIG. 12. Size distributions of fragments of basalt and pyrophyllite produced by impacts with the almost same P_I. Numbers indicate P_I values of each impact.

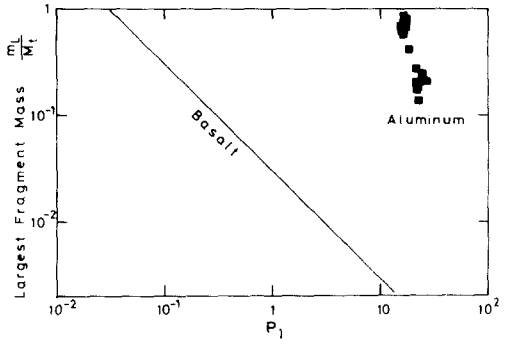

FIG. 13. The largest aluminum fragment mass normalized by the original projectile mass versus P_1. The solid line to the left indicates the least-squares fitting of the present experimental results for basalt.

orders of magnitude. This difference in the magnitude of P_1 is partly attributed to the fact that we used the compressive fracture strength for Y of basalt in Eq. (8), whereas we used the tensile yield strength for aluminum. However, the use of different strengths for basalt and aluminum explains only one order of magnitude difference observed for the two materials because the tensile strength of a rock is only about one order of magnitude smaller than the compressive strength. The essential difference between Figs. 11 and 13 probably lies in the fact that basalt is brittle and aluminum is ductile. The strain necessary to fracture the aluminum is orders of magnitude larger than that for basalt because of its ductility. For impact fracturing of a ductile material, we should use a scaling law different from that used for a brittle material, even if the new parameter of Mizutani *et al.*, P_1, is a useful scaling parameter. This result supports Matsui and Mizutani's (1977) suggestion that the ductility of metals has an important role in the formation of planets.

Impact Velocity Dependence of the Scaling Law

Impact pressure, P_0, in Eq. (5) is expressed in terms of the impact velocity by the equation (Mizutani *et al.*, 1983; 1984)

$$P_0 = \frac{1}{2}\xi\rho_{0T}C_T^2\left\{\left(\frac{v}{C_T}\right) + \frac{1}{2}s\xi\left(\frac{v}{C_T}\right)^2\right\} \quad (10)$$

where ρ_{0T} is the zero-pressure density of the target, C_T is the bulk-sound velocity of the target, and ξ is a factor related to the shock impedance ratio defined approximately by

$$\xi \simeq \frac{2\rho_{0P}C_P}{\rho_{0P}C_P + \rho_{0T}C_T}. \quad (11)$$

Using Eq. (11), the scaling law of Eq. (8) is approximated by

$$\frac{m_L}{M_t} \propto \left(\frac{L^3}{R^3}\right)^{-a_2}\left\{\left(\frac{v}{C_T}\right) + \frac{1}{2}s\xi\left(\frac{v}{C_T}\right)^2\right\}^{-a_2}. \quad (12)$$

Therefore the scaling law becomes, in the low-velocity range ($v \ll C_T$),

$$\frac{m_L}{M_t} \propto \left(\frac{L^3}{R^3}\right)^{-a_2}\left(\frac{v}{C_T}\right)^{-a_2} \quad (13)$$

and in the high-velocity range ($v \gg C_T$),

$$\frac{m_L}{M_t} \propto \left(\frac{L^3}{R^3}\right)^{a_2}\left(\frac{v}{C_T}\right)^{-2a_2}. \quad (14)$$

The latter equation is comparable to the conventional scaling law of Eq. (1),

$$\frac{m_L}{M_t} \propto \left(\frac{M_p v^2}{M_t}\right)^{-a_2}. \quad (15)$$

Because the data presented in this paper cover only the velocity range $v/C = 0.01$ to 1, the transition of Eq. (13) to Eq. (14) is not clear from the present data alone. But as discussed in detail in Mizutani *et al.* (1984), all the experimental data available, including those for ice (Lange and Ahrens, 1981) and glass (Gault and Wedekind, 1969), show that a single scaling of either Eq. (13) or Eq. (14) is not sufficient to describe the velocity dependence of the fragment size distribution. Further experimental studies in the velocity range $v/C > 1$ will be important in establishing the present scaling law of Eq. (12).

Size Distribution

In the previous section it was mentioned that the size distributions of fragments are

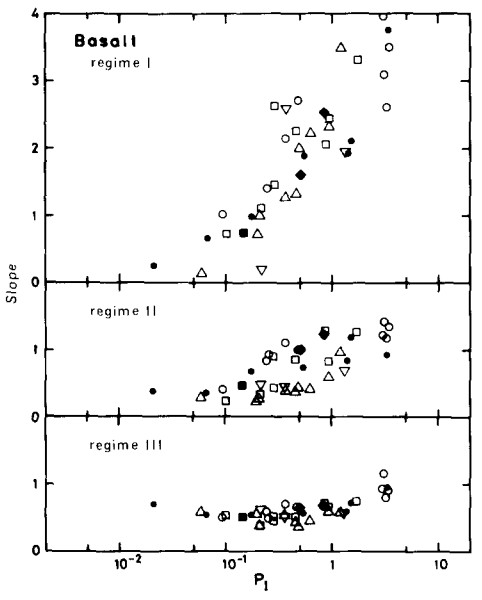

FIG. 14. Slopes of the log N–log m curve in each regime for basalts. Each symbol represents results with the same impact velocity range as that shown in Figs. 2 and 9.

divided into three regimes in the log N–log m plots. The slopes of the log N–log m curves in the three regimes are plotted against P_I in Fig. 14. It is evident that the slopes have positive correlations with P_I in regimes I and II. The slopes seem to be expressed by the expression

$$a = C_3 + a_3 \log P_I \qquad (16)$$

where a is the slope of the size distribution in the log N–log m diagram. Least-squares fitting of experimental results for basalts gives the values of C_3 and a_3 in Table V. In regime III, the slope is almost constant at 0.5–0.6 in the range $P_I < 1$ but it seems to increase gently in the range of $P_I > 1$ as P_I increases.

As for the experimental results for pyrophyllites, the least-squares fitting also determines the coefficients of Eq. (16), which are listed in Table V. Considering the rather large uncertainty of the estimated C_3 and a_3, parameters for pyrophyllite are thought to be almost identical to those for basalt, respectively. This indicates that the parameters for basalt are representative of the size distributions of rocky fragments produced by high-velocity impacts.

These results indicate to us that the impact condition is learned from the size distribution of fragments produced by a high-velocity impact. If the size distribution of an asteroid family keeps the original size distribution of fragments which might have been produced by a high-velocity impact, important information on the impact will be obtained by using the present scaling law for fragment size distributions. Although a detailed discussion of the application of the present experiment to the asteroid size distribution will be made elsewhere, we briefly compare in Fig. 15 the present experimental results with the asteroid size distribution of the Flora family. The volume of each asteroid was calculated assuming the shape of the asteroid is spherical. The radii of asteroids are estimated from TRIAD data (Bowell *et al.*, 1979) using the standard formula (Zellner, 1979) and assuming that the color excess, B–V, and visual albedo, p_v, are 0.84 and 0.129, respectively (Bowell *et al.*, 1979). Detection bias correction, which will probably be necessary for the size range smaller than 10^{12} m^3, is not made.

The size distribution of the Flora family shows three regimes similar to the curves

TABLE V

THE RESULTS OF THE LEAST-SQUARES FITTING OF THE EXPERIMENTAL DATA ON SIZE DISTRIBUTIONS WITH EQ. (16)—PRESENT STUDY

	$a = C_3 + a_3 \log P_I$		
	C_3[a]	a_3[a]	σ[b]
Basalt			
Regime I	2.43 (0.14)	1.56 (0.23)	0.73
Regime II	0.90 (0.05)	0.51 (0.08)	0.24
Pyrophyllite			
Regime I	2.19 (0.27)	1.62 (0.45)	0.49
Regime II	0.79 (0.06)	0.59 (0.10)	0.11

[a] Numbers in parentheses are standard deviations of the estimated parameters.

[b] $\sigma = \sqrt{\Sigma\{a_{exp} - a_{theor}\}^2/N}$.

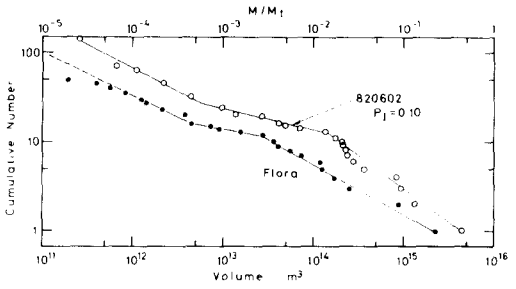

FIG. 15. Size distributions of an asteroid family and the present experimental results.

obtained in the present experiments, though some of the other families do not clearly show the third regime because of the small numbers of asteroids from which the radii were determined and the similarity in slope of the size distributions in regimes II and III. From the slopes of the size distribution of members in the Flora family in regimes I–III, we can estimate the nondimensional impact stress, P_I, using the presently obtained scaling law of Eq. (16). The estimated value of P_I is 0.05 to 0.15. In the same way we can estimate the P_I values for the Themis, Eos, and Koronis families. They are 0.02–0.09, 0.1–0.6, and 0.2–0.9, respectively. From the above-estimated P_I value, we can estimate the original volume of the parent body of the family using Eq. (9). The estimated m_L/M_t ratio of 0.6 to 0.2 for the Flora family indicates that the volume of the parent body of the Flora family is 1.6 to 5 times as large as that of the largest member (8 Flora) of the Flora family. It is approximately equal to the total volume of the asteroids shown in Fig. 15 (2.0 times 8 Flora's volume). The discussion above is just a simple application of the present scaling law to the size distribution of asteroids but it may serve to illustrate how the present scaling law is useful for interpretation of various planetary problems.

CONCLUSION AND SUMMARY

Impact fragmentation experiments were performed on basalts and pyrophyllite. Comparing the present experimental data with those from previous studies, we found that the P_I introduced by Mizutani *et al.* (1984) is a useful parameter to describe impact fragmentation phenomena. The following quantities are expressed by nearly identical power laws of P_I for both basalts and pyrophyllites:

(1) the largest fragment mass (m_L) normalized to the original target mass (M_t), when the destroyed material is brittle,

$$m_L/M_t \propto P_I^{-1};$$

(2) the slopes of log N–log m curves in the regime of large- and medium-range size distributions,

$$N(m/M_t) \propto (m/M_t)^{-\{C_3 + a_3 \log P_I\}}.$$

These results show that fragment size and fragment size distributions form a record of impact conditions. Because parameter P_I is derived from three independent pieces data such as the largest fragment size and the slopes of the size distribution in regimes I and II, we can estimate it with some confidence. Since P_I is a combination of impact velocity, ratio of projectile size to target size, and target strength, any one of these quantities is deduced if the others are estimated by other independent methods.

ACKNOWLEDGMENTS

It is a pleasure to acknowledge the invaluable technical help and interesting discussions of M. Kumazawa and M. Kato. We also acknowledge two anonymous reviewers for their careful reading of the manuscript.

REFERENCES

BOWELL, E., T. GEHRELS, AND B. ZELLNER (1979). Magnitudes, colors, types and adopted diameters of the asteroids. In *Asteroids* (T. Gehrels, Ed.), pp. 1014–1039. Univ. of Arizona Press, Tucson.

DIENES, J. K., AND J. M. WALSH (1970). Theory of impact: Some general principles and the method of Eulerian codes. In *High-Velocity Impact Phenomena* (R. Kinslow, Ed.), pp. 25–104. Academic Press, New York.

FUJIWARA, A., G. KAMIMOTO, AND A. TSUKAMOTO (1977). Destruction of basaltic bodies by high velocity impact. *Icarus* **31**, 277–288.

FUJIWARA, A., AND A. TSUKAMOTO (1980). Experimental study on the velocity of fragments in collisional breakup. *Icarus* **44,** 142–153.

GAULT, D. E., AND J. A. WEDEKIND (1969). The destruction of tektites by micrometeoroid impact. *J. Geophys. Res.* **74,** 6780–6794.

GEHRING, J. W., JR. (1970). Engineering considerations in hypervelocity impact. In *High-Velocity Impact Phenomena* (R. Kinslow, Ed.), pp. 463–514. Academic Press, New York.

GRIFFITH, A. A. (1920). The phenomena of rupture and flow in solids. *Philos. Trans. R. Soc. London Ser. A* **221,** 163–198.

HARTMANN, W. (1978). Planet formation: Mechanism of early growth. *Icarus* **33,** 50–61.

KAWAKAMI, S., H. MIZUTANI, Y. TAKAGI, M. KATO, AND M. KUMAZAWA (1983). Impact experiments on ice. *J. Geophys. Res.* **88,** 5806–5814.

LANGE, A., AND T. J. AHRENS (1981). Fragmentation of ice by low velocity impact. *Proc. Lunar Planet. Sci. Conf. 12th,* 1667–1687.

LANGE, A., AND T. J. AHRENS (1982). Impact fragmentation of ice–silicate bodies. In *Lunar and Planetary Science XIII,* pp. 417–418. Lunar and Planetary Institute, Houston.

MATSUI, T., AND H. MIZUTANI (1977). Why is a minor planet minor? *Nature* **270,** 506–507.

MATSUI, T., T. WAZA, K. KANI, AND S. SUZUKI (1982). Laboratory simulation of planetesimal collisions. *J. Geophys. Res.* **87,** 10,968–10,982.

MCQUEEN, R. G., S. P. MARSH, J. W. TAYLOR, J. N. FRITZ, AND W. J. CATER (1970). The equation of state of solids from shock wave studies. In *High-Velocity Impact Phenomena* (R. Kinslow, Ed.), pp. 25–104. Academic Press, New York.

MIZUTANI, H., M. KUMAZAWA, M. KATO, T. MASUDA, S. KAWAKAMI, Y. TAKAGI, AND K. KANI (1981). Performance tests of the high velocity shock gun with a novel sabot stopper. *Proc. ISAS Lunar Planet. Sci. Symp. 14th,* 267–277.

MIZUTANI, H., S. KAWAKAMI, Y. TAKAGI, M. KATO, AND M. KUMAZAWA (1983). Cratering experiments in sands and a trial for general scaling law. *J. Geophys. Res.* **88**(Suppl.), A835–A845.

MIZUTANI, H., Y. TAKAGI, AND S. KAWAKAMI (1984). New scaling law on impact fragmentation. In preparation.

PATERSON, M. S. (1978). *Experimental Rock Deformation—The Brittle Field.* Springer-Verlag, New York/Berlin.

RINEHART, J. S. (1975). *Stress Transients in Solids.* HyperDynamics, Santa Fe.

RUOFF, A. L. (1967). Linear shock-velocity–particle-velocity relationship. *J. Appl. Phys.* **38,** 4976–4980.

TAKAGI, Y. (1983). *Fragmentation Experiments of Basalt, Size and Velocity Distributions of Fragments.* Master's thesis, Nagoya University.

ZELLNER, B. (1979). Asteroid taxonomy and the distribution of the compositional types. In *Asteroids* (T. Gehrels, Ed.), pp. 783–806. Univ. of Arizona Press, Tucson.